

# Bottomonia in the Quark-Gluon Plasma and their Production at RHIC and LHC

A. Emerick

*School of Physics and Astronomy, University of Minnesota, Minneapolis, MN 55414, USA*

X. Zhao

*Department of Physics and Astronomy, Iowa State University, Ames, IA 50011, USA*

R. Rapp

*Cyclotron Institute and Department of Physics&Astronomy,  
Texas A&M University, College Station, TX 77843-3366, USA*

(Dated: November 7, 2018)

We study the production of bottomonium states in heavy-ion reactions at collider energies available at RHIC and LHC. We employ an earlier constructed rate equation approach which accounts for both suppression and regeneration mechanisms in the quark-gluon plasma (QGP) and hadronization phases of the evolving thermal medium. Our previous predictions utilizing two limiting cases of strong and weak bottomonium binding in the QGP are updated by (i) checking the compatibility of the pertinent spectral functions with lattice-QCD results for euclidean correlators, (ii) adapting the initial conditions of the rate equation by updating bottom-related input cross sections and the charged-particle multiplicity of the fireball, and (iii) converting our calculations into observables as recently measured by the STAR and CMS experiments. Our main findings are a preference for strong  $\Upsilon$  binding as well as a significant regeneration component at the LHC.

## I. INTRODUCTION

Quarkonia by now have a 25-year history of being utilized as a probe of the Quark-Gluon Plasma (QGP) in ultrarelativistic heavy-ion collisions (URHICs), cf. Refs. [1–3] for recent reviews. The majority of the studies to date have been devoted to charmonium properties and their observable consequences in experiment, with few exceptions for bottomonia [4–9]. Recently, experiments at the Large Hadron Collider (LHC) [10, 11] and the Relativistic Heavy-Ion Collider (RHIC) [12] have measured  $\Upsilon$  mesons in URHICs for the first time, and subsequent phenomenological analyses have commenced [13, 14], focusing on suppression mechanisms in Pb-Pb( $\sqrt{s}=2.76$  ATeV) in comparison to CMS data. For charmonia, regeneration effects due to coalescence of  $c$  and  $\bar{c}$  quarks have complicated the interpretation of observables appreciably. Since the cross section for open bottom is much smaller than for open charm, regeneration of bottomonia has been argued to be negligible. This would render bottomonium production in URHICs a more pristine probe of quarkonium dissolution in the QGP. However, quantitative estimates [7, 8] indicate that this may not be the case. The magnitude of the regeneration contribution depends on a subtle interplay of the masses of the open- and hidden-bottom states in a system with fixed  $b\bar{b}$  content. In addition, the ratio of hidden- to open-bottom states in elementary hadronic collisions is typically of order 0.1% – and thus much smaller than in the charm sector where it is around 1% –, implying that even small contributions to bottomonium regeneration can be significant relative to primordial production. Furthermore, a consistent interpretation of bottomonium production in URHICs should encompass both LHC and RHIC data.

The above aspects were addressed in previous work [7]

where predictions for the nuclear modification factor,  $R_{AA}$ , of inclusive  $\Upsilon$  production at RHIC and LHC have been presented. Unfortunately, these calculations could not be directly mapped to the now available data: at RHIC the  $R_{AA}$  for the sum of 1S, 2S and 3S states has been measured, and at LHC the current data are taken at half of the design energy,  $\sqrt{s}=2.76$  ATeV. Furthermore, the availability of bulk-hadron observables in Pb-Pb collisions at the LHC helps to constrain the fireball model in terms of its total entropy and transverse expansion which govern the temperature evolution, thus affecting bottomonium suppression and regeneration. Calculations of the latter also benefit from an updated input for the bottom(onium) cross sections (if only suppression is considered, this input cancels out in the suppression factor). We also improve the theoretical input to the earlier calculations by applying theoretical constraints on the in-medium bottomonium properties (binding energy and dissociation width) in terms of euclidean correlators computed in recent years within thermal lattice-QCD (lQCD) [15–17]. In Ref. [7], two scenarios for in-medium bottomonia were discussed, i.e., one with vacuum and one with in-medium binding energies estimated from a screened Cornell potential [18]. With the now available lattice data, we can refine the pertinent spectral functions following the approach outlined in Ref. [19].

Our paper is organized as follows. In Sec. II we revisit the spectral properties of bottomonia in an equilibrated QGP within two limiting scenarios, “strong” and “weak” binding, and check the resulting euclidean correlators against lQCD data. In Sec. III we briefly recall the kinetic rate-equation framework in a thermal medium and discuss its (suitably updated) input quantities. In Sec. IV we present the updated results on bottomonium production at RHIC and LHC, focusing on its central-

ity dependence in comparison to STAR and CMS data. We evaluate our results and put them into context with existing calculations. In Sec. V we summarize and conclude.

## II. BOTTOMONIUM SPECTRAL FUNCTIONS IN THE QUARK-GLUON PLASMA

Following Ref. [7] we attempt to bracket the properties of bottomonia in the QGP by defining two scenarios for the temperature dependence of their binding energy,

$$\epsilon_B(T) = 2m_b(T) - m_Y \quad (1)$$

( $m_b(T)$ : in-medium bottom mass;  $m_Y$ : bottomonium bound-state mass with  $Y = \Upsilon(1S), \Upsilon(2S), \chi_b(1P), \dots$ ). These are:

1. Weak Binding Scenario (WBS): bottomonium bound-state energies are significantly reduced in the QGP, relative to the vacuum state, adopting the screened Cornell-potential results of Ref. [18]. The bound state masses are kept at their vacuum value which is motivated by the approximate constancy of their in-medium correlator ratios as found in lQCD (further details below). This, in turn, requires the in-medium bottom quark-threshold to decrease with increasing temperature (which is not inconsistent with independent lQCD computations of the heavy-quark free energy).
2. Strong Binding Scenario (SBS): the temperature dependence is removed from Eq. (1), implying bound states to remain at their vacuum mass and binding energy throughout the QGP, with a constant open-bottom threshold at  $2m_b = 2m_B = 10.56$  GeV.

Figure 1 shows the temperature dependences of  $\epsilon_B$  for the ground state  $\Upsilon$ , for  $\Upsilon'$  and  $\chi_b(1P)$ , within these two scenarios. The constant values in the SBS are to be contrasted with factor of at least 2 reduction at  $T_c=180$  MeV (and rapidly decreasing further with  $T$ ) in the WBS. Strong- and weak-binding scenarios also emerge in potential-model calculations, due to current uncertainties in defining the in-medium interaction kernel, usually bracketed by the internal and free energies of the  $Q\bar{Q}$ , see, e.g., Ref. [20]. In the present context we are not (yet) aiming at a quantitative implementation of potential-model results, but rather at exploring the sensitivity of heavy-ion data to  $Y$  spectral properties within the two cases defined above.

The next step is the evaluation of the  $Y$  dissociation widths. For a Coulombic bound state with large binding energy,  $\epsilon_B \gg \Lambda_{\text{QCD}}$ , the leading break-up mechanism has been identified and calculated more than 30 years ago as the gluo-dissociation process,  $g + Q \rightarrow Q + \bar{Q}$  ( $Q$ : quarkonium) [21]. The corresponding cross section is peaked around incoming gluon energies of  $k_0 = (10/7)\epsilon_B$ .

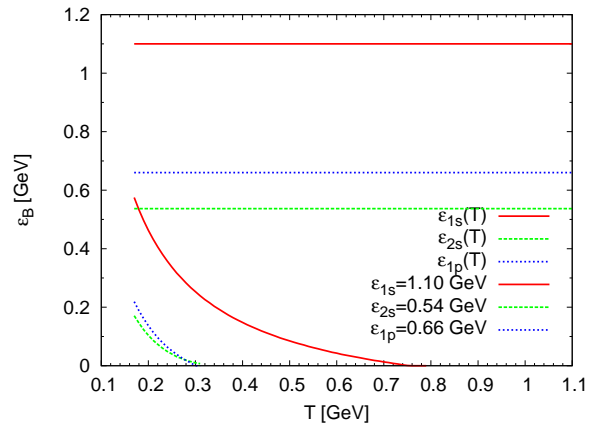


FIG. 1: Temperature dependence of the binding energies,  $\epsilon_B(T)$ , for  $\Upsilon$  (solid lines),  $\Upsilon'$  (dotted lines) and  $\chi_b$  (dashed lines) in the Strong- and Weak-Binding scenarios (upper and lower 3 lines, respectively).

For weakly bound quarkonia,  $\epsilon_B \leq T$ , this mechanism becomes inefficient and is supplanted by the quasifree break-up,  $p + Q \rightarrow p + Q + \bar{Q}$  ( $p = g, q, \bar{q}$ ) [22]. This picture has been well established by now. For example, in effective-field-theory approaches to quarkonia, the gluo-dissociation corresponds to the so-called “singlet-to-octet” transitions [23, 24] while the quasifree mechanism corresponds to Landau damping in the gluon-exchange potential [23, 25]. Accordingly, we will treat the SBS with the gluo-dissociation and the WBS with the quasifree mechanism. The pertinent dissociation rates (inelastic widths) can be expressed in terms of an underlying cross section,  $\sigma_Y^{\text{diss}}$ , convoluted over the thermal parton distribution functions,  $f^p$ , as

$$\begin{aligned} \Gamma_Y^{\text{diss}}(q; T) &\equiv \tau_Y^{-1}(q; T) \\ &= \sum_{p=q, \bar{q}, g} \int \frac{d^3k}{(2\pi)^3} f^p(\omega_k; T) \sigma_Y^{\text{diss}}(s) v_{\text{rel}} \quad (2) \end{aligned}$$

where  $\omega_k$  denotes the on-shell energy of a parton with 3-momentum  $k$ , and  $s = (k^{(4)} + q^{(4)})^2$  is the total center-of-mass energy squared in the collision with a  $Y$  of 3-momentum  $q$  ( $v_{\text{rel}}$  is their relative velocity). The bottomonium lifetimes are plotted in Fig. 2 for  $\vec{q} = 0$ , for  $\Upsilon$ ,  $\Upsilon'$  and  $\chi_b$  in the weak- and strong-binding scenarios (left and right panel, respectively). As in Ref. [7] quasifree dissociation is calculated with  $\alpha_s \simeq 0.26$ , while for gluo-dissociation a Coulomb-like binding for  $\Upsilon(1S)$  with  $\epsilon_B = 1.1$  GeV translates into an effective coupling of  $\alpha_s \simeq 0.65$ . Within the WBS, quasifree dissociation induces little difference between the  $\Upsilon'$  and  $\chi_b$  widths, due to their almost identical (small) binding energies. The  $\Upsilon(1S)$  lifetime is about an order of magnitude longer than for the excited states at  $T_c$ , but quickly approaches their lifetimes since  $\epsilon_B$  decreases to small values at higher temperature. In the SBS gluo-dissociation produces a larger spread in the lifetimes of ground and excited states. At

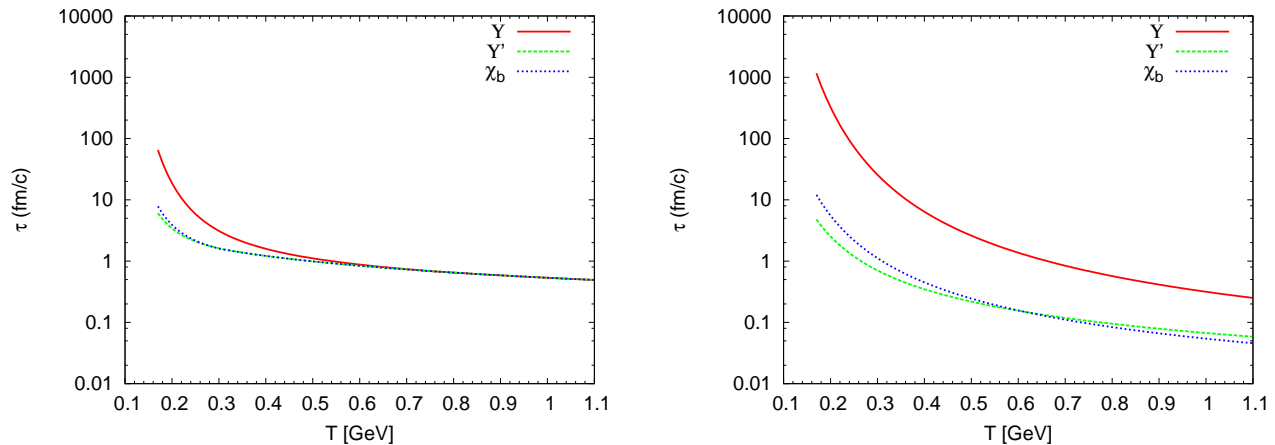


FIG. 2: Bottomonium lifetimes in the QGP for the two binding scenarios defined in the text; left panel: WBS with quasifree dissociation; right: SBS with gluo-dissociation; solid lines:  $\Upsilon$ , dashed lines:  $\Upsilon'$ , dotted lines:  $\chi_b$ .

$T_c$ , the  $\Upsilon(1S)$  lifetime is by almost two orders of magnitude larger than its WBS counterpart, but it comes close to the latter at high temperatures,  $T \simeq 1$  GeV. However, it stays well above the lifetimes of the excited states even at high  $T$ . Close to  $T_c$ , the lifetimes of the excited states in the SBS are quite comparable to their WBS counterparts, even dropping below the latter for  $T \geq 250$  MeV or so. The reason for that is the larger coupling in the SBS together with a favorable overlap of the typical thermal gluon energies,  $\bar{\omega}_k \simeq 3T$ , with the maximum in the gluo-dissociation cross sections around  $\omega_k \sim \epsilon_B \simeq 600$  MeV. Thus, for the phenomenologically relevant temperatures, especially at RHIC, one expects the suppression factors of the excited states to be similar in the SBS and WBS.

With the masses and widths (real and imaginary parts of the inverse propagator) of the  $Y$  bound states determined we proceed to compute the pertinent spectral functions. We follow Ref. [19] for the charmonium case by adopting an ansatz consisting of a relativistic Breit-Wigner (RBW) for the bound-state part and a nonperturbative continuum for energies above the  $b\bar{b}$  threshold. We neglect the excited states of  $Y$ . One has

$$\sigma_Y(\omega) = A_Y \frac{2\omega}{\pi} \frac{Z_Y \omega \Gamma_Y(T)}{(\omega^2 - m_Y^2)^2 + \omega^2 \Gamma_Y(T)^2} + \frac{B_Y N_c}{8\pi^2} \Theta(\omega^2 - s(T)) \omega^2 \sqrt{1 - \frac{s(T)}{\omega^2}} \left( a + b \frac{s(T)}{\omega^2} \right), \quad (3)$$

where  $N_c=3$  is the number of colors,  $A_Y$  is given by the wave function overlap at the origin in vacuum,  $Z_Y$  characterizes its modification in medium (“polestrength”),  $s(T) = 2m_b(T)$  marks the in-medium  $b\bar{b}$  threshold following Eq. (1), and the coefficients  $(a, b)$  arise from the Dirac structure specific to the hadronic channel under consideration, e.g., (2,1) for the vector channel. The prefactor  $B_Y = 2$  augments the perturbative expression of the continuum to account for  $b\bar{b}$  rescattering effects and is estimated from the  $T$ -matrix calculations of Ref. [20]. We approximate the total width for the bound state with its

dissociation rate (inelastic width). Figure 3 shows the in-medium  $\Upsilon$  spectral function for two temperatures in the WBS and SBS. One clearly recognizes the much larger width and reduced threshold in the WBS compared to the SBS. In the latter the  $b\bar{b}$  threshold remains constant at  $\sqrt{s} = 10.56$  GeV.

In a final step we check the above spectral function against results from thermal IQCD where the bottomonium correlators,  $G(\tau)$ , are computed as a function of euclidean time  $\tau$ . The euclidean correlator is related to the spectral function as

$$G_\alpha(\tau; T) = \int_0^\infty d\omega \sigma_\alpha(\omega; T) K(\omega, \tau; T), \quad (4)$$

where  $\alpha$  specifies the hadronic channel, and the kernel reads

$$K(\omega, \tau; T) = \frac{\cosh[\omega(\tau - 1/2T)]}{\sinh[\omega/2T]}. \quad (5)$$

To better exhibit the medium effects, it is common to consider the correlator ratio,

$$R_G(\tau; T) = \frac{G_\alpha(\tau, T)}{G_\alpha^{rec}(\tau, T)}, \quad (6)$$

where the denominator is evaluated with the same kernel but with a spectral function evaluated at a low (or zero) temperature,  $T^*$ , where no significant medium effects are expected. To compute the euclidean correlator ratios for our in-medium spectral functions we define a vacuum spectral function using Eq. (3) in the narrow-width limit and with  $Z_Y=1$  for the RBW part and with  $\sqrt{s} = 2m_B = 10.56$  GeV for the continuum (as for the in-medium spectral function, we only include the ground state). Our results for  $R_G(\tau, T)$  are displayed in Fig. 4. In the strong-binding scenario (featuring vacuum binding energies and  $b\bar{b}$  threshold), the only medium effect is

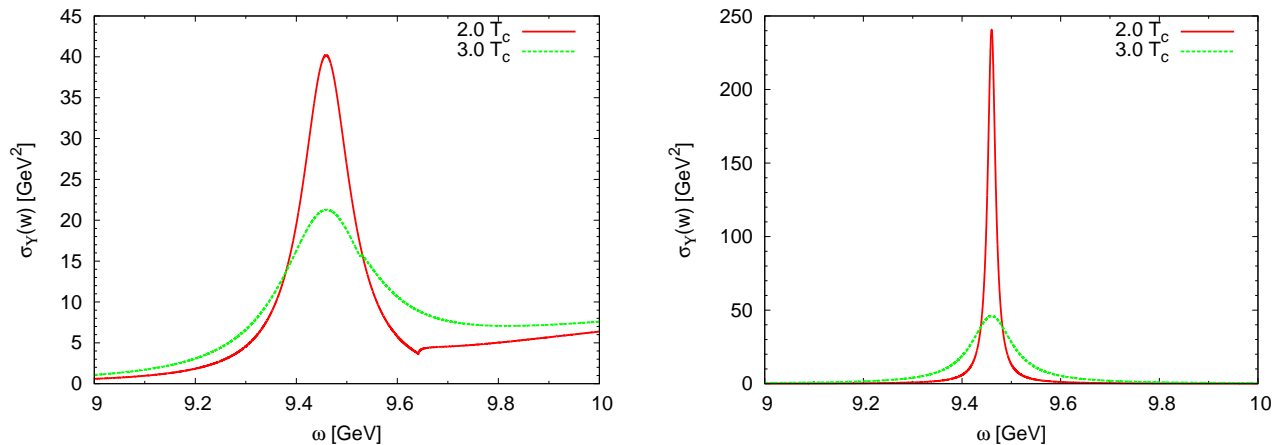


FIG. 3: Spectral functions of the  $\Upsilon$  calculated from Eq. (3) in a QGP of temperatures  $2T_c$  (solid lines) and  $3T_c$  (dashed lines); left panel: weak-binding scenario, right panel: strong binding scenario.

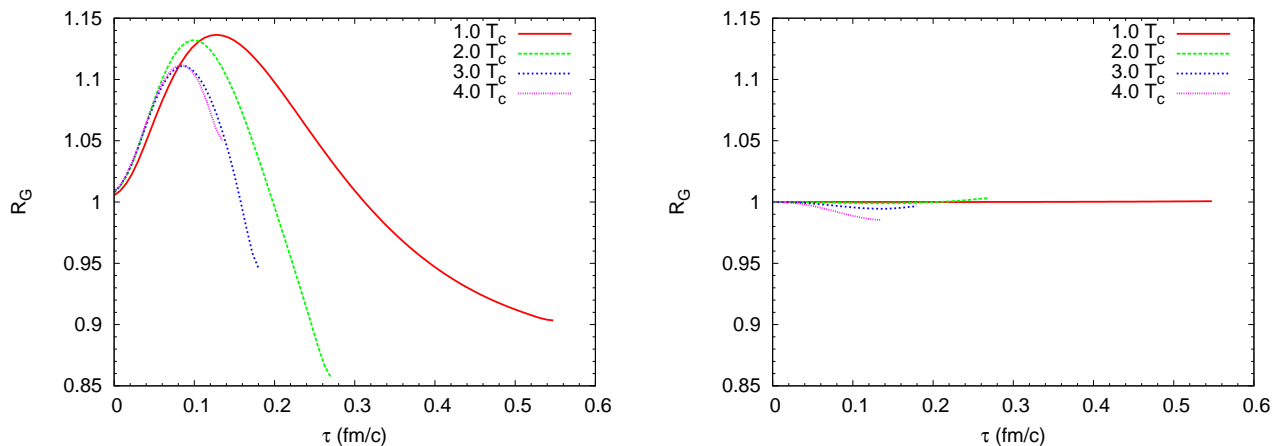


FIG. 4: Euclidean correlator ratios following from the in-medium  $\Upsilon$  spectral functions shown in Fig. 3 at various temperatures for the weak-binding (left panel) and strong-binding scenario (right panel).

the increasing decay width, which, however, has very little impact on the correlator ratio so that the latter stays within 2% of one up to the highest temperature considered ( $4T_c$ ), cf. right panel of Fig. 4. In the weak-binding scenario, the bound-state mass is also constant, but the threshold energy drops appreciably, which by itself would imply an increase of  $R(\tau)$  above one. However, a weakening bound state is not only characterized by a reduction in  $\epsilon_B$  but also by a reduction of its polestrength (see, e.g., Ref. [20]), which is represented by the  $Z_Y$ -factor in the RBW. We have tuned this quantity to recover  $R(\tau)$  at around one resulting in the curves shown in the left panel of Fig. 4. The deviations from one are larger in the WBS compared to the SBS, comparable to what has been found for charmonia with the same ansatz [19]. The SBS, therefore, appears to be a more natural realization of the near-constancy of  $R(\tau) \simeq 1$  at the few-percent level as found in thermal lQCD [15–17]. This insight is one of the main motivations for re-evaluating the previ-

ous phenomenological analysis of Ref. [7] where the in-medium binding scenario with quasifree dissociation was believed to be more realistic for bottomonia in the QGP. To our knowledge, this has not been done in any other phenomenological application thus far.

### III. KINETIC-THEORY MODEL

In this section we first set up the rate-equation framework for the  $Y$  states in the expanding QGP (Sec. III A), followed by specifying the inputs and initial conditions for their numerical evaluation, specifically

- (i) the temperature and volume evolution of the thermal bulk medium (Sec. III B), and
- (ii) the initial conditions for the various  $Y$  states and the number of  $b\bar{b}$  pairs in the system (Sec. III C).

## A. Rate Equation

To simulate the evolution of the bottomonium abundances in URHICs at RHIC and LHC we adopt the rate-equation approach of Ref. [26] (also used in Ref. [7]). It describes the approach of the number,  $N_Y$ , of bottomonium state  $Y$ , toward equilibrium as

$$\frac{dN_Y}{d\tau} = -\Gamma_Y^{\text{diss}}(T) [N_Y - N_Y^{\text{eq}}(T)] . \quad (7)$$

The key quantities in this equation are the inelastic reaction rate,  $\Gamma_Y^{\text{diss}}$ , and the equilibrium limit,  $N_Y^{\text{eq}}$ , which directly relate to the spectral properties discussed in the previous section. The inelastic reaction rate would be all that is needed if only suppression effects were considered, governed by the first (loss) term on the right-hand-side of Eq. (7). Regeneration processes are accounted though the gain term,  $\Gamma_Y^{\text{diss}}(T)N_Y^{\text{eq}}(T)$ . Its form is dictated by the detailed balance between the dissociation and regeneration processes. Apart from the inelastic reaction rate, the gain term is controlled by the equilibrium limit which is computed as follows. For a given collision energy, system and centrality, the total number of  $b\bar{b}$  pairs is assumed to be constant throughout the evolution of the expanding fireball. Assuming relative chemical equilibrium between all available states containing bottom quarks at given temperature and volume of the system, the  $b\bar{b}$  number is matched to the equilibrium numbers of bottom states by the condition

$$N_{b\bar{b}} = \frac{1}{2} N_{\text{op}} \frac{I_1(N_{\text{op}})}{I_0(N_{\text{op}})} + N_{\text{hid}} , \quad (8)$$

by means of a  $b$ -quark fugacity factor,  $\gamma_b \equiv \gamma_{\bar{b}}$ . The equilibrium open- and hidden-bottom numbers in the QGP are given by

$$N_{\text{op}} = \gamma_b V_{\text{FB}} d_b \int \frac{d^3p}{(2\pi)^3} f^b(p; T) \quad (9)$$

$$N_{\text{hid}} = \gamma_b^2 V_{\text{FB}} \sum_Y d_Y \int \frac{d^3p}{(2\pi)^3} f^Y(p; T) , \quad (10)$$

and  $V_{\text{FB}}$  is the fireball volume at given temperature,  $T(\tau)$ . The equilibrium number densities are simply those of  $b$  quarks (with spin-color and particle-antiparticle degeneracy  $d_b=6 \times 2$ ) and bottomonium states (summed over including their spin degeneracies,  $d_Y$ ). They are calculated using the same in-medium masses for open- and hidden-bottom states as in the spectral function analysis in Sec. II for both the SBS and WBS, respectively. At fixed  $N_{b\bar{b}}$  a large  $b$ -quark mass leads to a large  $\gamma_b$  which in turn results in a large equilibrium number,  $N_Y$ . This is reflected in the temperature dependence of the  $\Upsilon$  equilibrium numbers which are much larger in the strong-binding scenario, cf. Fig. 5. The ratio of modified Bessel functions,  $I_1(N_{\text{op}})/I_0(N_{\text{op}})$ , in Eq. (8) enforces exact conservation of the net  $b$  number in each event (canonical ensemble).

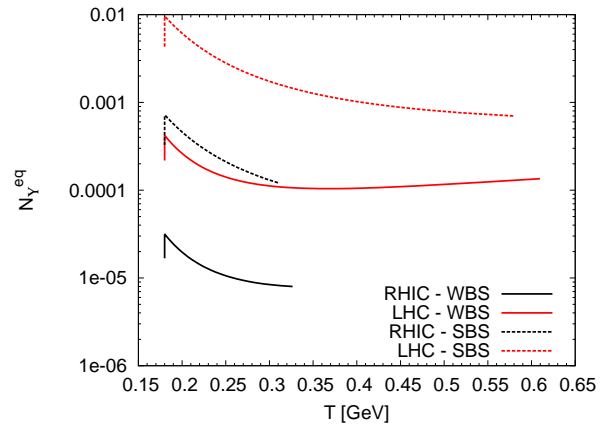


FIG. 5: Equilibrium numbers of  $\Upsilon$  vs. temperature at RHIC ( $\sqrt{s_{NN}} = 0.2$  TeV, lower two lines) and LHC ( $\sqrt{s_{NN}} = 2.76$  TeV, upper two lines) using equation (10) with bottom-production cross sections as specified in Sec. III C below. The solid lines correspond to the weak-binding scenario (with in-medium  $b$ -quark mass) and the dashed lines to the strong-binding scenario (with vacuum  $b$ -quark mass).

In heavy-ion collisions, however,  $b$ -quarks are not expected to *kinetically* equilibrate [27]. Bottom-quark spectra which are harder than in equilibrium imply less phase-space overlap between  $b\bar{b}$  pairs and thus a reduced  $Y$  regeneration. To account for this we follow Ref. [28] by introducing a relaxation-time factor

$$\mathcal{R}(\tau) = 1 - \exp\left(1 - \int_{\tau_0}^{\tau} \frac{d\tau'}{\tau_{\text{eq}}}\right) \quad (11)$$

whose timescale is set by the kinetic relaxation time,  $\tau_{\text{eq}}$ , of  $b$  quarks in the QGP. In our calculations it is taken as  $\tau_{\text{eq}} \simeq 10$  fm/ $c$  around  $T \simeq 2T_c$ , in a range consistent with microscopic  $T$ -matrix calculations of bottom diffusion [20] (with these diffusion coefficients a fair description of the observed open heavy-flavor suppression and elliptic flow at RHIC is possible [29]).

## B. Fireball Model

Our fireball model has been updated compared to Ref. [7] by matching it to our recent charmonium applications at RHIC [19] and LHC [30]. We assume an isentropically expanding isotropic firecylinder whose eigenvolume is approximated by the ansatz

$$V_{\text{FB}}(\tau) = (z_0 + v_z \tau) \pi \left( r_0 + \frac{1}{2} a_{\perp} \tau^2 \right)^2 , \quad (12)$$

with initial transverse radius,  $r_0$ , longitudinal velocity  $v_z=1.4c$  and transverse acceleration  $a_{\perp}=0.1c^2/\text{fm}$ . The latter is larger than in Ref. [7] to better reproduce measured bulk-hadron  $p_t$  spectra and leads to a slight reduction in the QGP and mixed-phase lifetime. At each



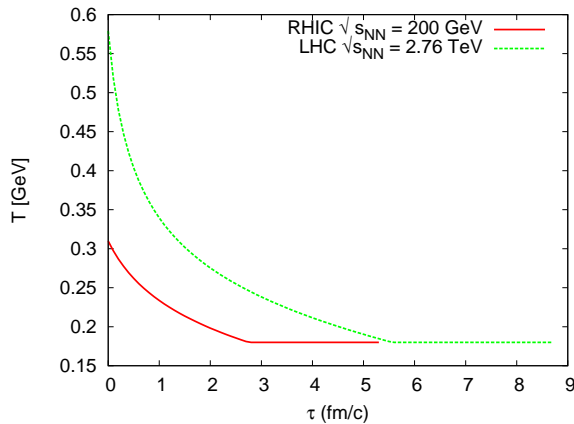


FIG. 6: Temperature evolution of the fireball model at RHIC (solid line) and LHC (dotted line). At RHIC the evolution is given for central Au-Au collisions at  $\sqrt{s_{NN}}=0.2$  TeV and a QGP formation time  $\tau_0 = 0.6$  fm/c; at LHC the evolution is for central Pb-Pb collisions at  $\sqrt{s_{NN}}=2.76$  TeV and  $\tau_0 = 0.20$  fm/c.

centrality and collision energy of a heavy-ion collision, the total entropy,  $S$ , is chosen to reproduce the observed charged-hadron multiplicity (computed with a hadron resonance gas at a chemical freezeout temperature,  $T_{ch}=T_c=180$  MeV). With  $S = 10000(22000)$  for  $N_{part}=375$  nucleon participants at RHIC (LHC) one obtains  $dN_{ch}/dy=800(1750)$ . The entropy density,  $s(\tau) = S/V_{FB}(\tau)$ , is used to determine the temperature,  $T(\tau)$ , by means of a QGP quasiparticle equation of state for  $s(T)$ . At  $T=T_c$  a standard mixed-phase construction is employed. We have verified that the impact of the subsequent hadronic evolution (also in the mixed phase) is negligible for all  $Y$  states. The initial longitudinal length,  $z_0 = \tau_0 \Delta y$ , controls the initial temperature ( $\Delta y = 1.8$  is the rapidity coverage of the fireball). With the QGP formation time  $\tau_0 = 0.6(0.2)$  fm/c one obtains  $T_0 = 330(610)$  MeV at RHIC (LHC). The temperature evolution of the fireball for central collisions is displayed in Fig.6, with QGP and mixed phases indicated.

### C. Primordial $Y$ and Bottom Yields

The rate equation requires an initial condition for the number of bottomonia at the QGP formation time,  $N_Y(\tau_0)$ . We determine these by using their production cross section in  $pp$  collisions and binary collision ( $N_{coll}(b)$ ) scaling in AA collisions. We use inelastic NN cross sections of  $\sigma_{pp}^{inel}=42$  mb and 62 mb at  $\sqrt{s}=0.2$  and 2.76 TeV, respectively. In addition, we allow for cold-nuclear-matter (CNM) suppression, collectively defined as being due to modifications of  $N_Y$  prior to thermalization, most notably nuclear modifications of the parton distribution functions, absorption on passing-by primordial nucleons (or even secondary particles), and the

Quantity	$\sqrt{s_{NN}}=0.2$ TeV	Ref.	$\sqrt{s_{NN}}=2.76$ TeV	Ref.
$\sigma_{pp}^{inel}$ [mb]	42	[32]	62	[32]
$\sigma_{pp \rightarrow \Upsilon}^{inc}$ [nb]	6.6	[33]*	$250 \pm 30$	[34]*
$\sigma_{pp \rightarrow \Upsilon}^{dir}$ [nb]	3.4	[33]*	128	[35]*
$\sigma_{pp \rightarrow \Upsilon'}^{dir}$ [nb]	2.2	[33]*	83	[35]*
$\sigma_{pp \rightarrow \chi_b}^{dir}$ [nb]	7.1	[33]*	270	[35]*
$\sigma_{pp \rightarrow b\bar{b}}^{tot}$ [ $\mu$ b]	$3.2 \pm 1.8$	[37]*	$142 \pm 25$	[38]*
$R_y$	0.52	[40]	0.3	[40]
$S(N_p=375)$	10000	[22]	22000	[30]
$\tau_0$ [fm/c]	0.6	[19]	0.2	[30]

TABLE I: Summary of cross sections in  $pp$  collisions used to initialize the hidden- and open-bottom abundances of our rate equations in Au-Au at RHIC (second column) and Pb-Pb at LHC (fourth column). Uncertainties are quoted when quantitatively available; starred references require further explanation, given in the text.

Cronin effect. For simplicity, we approximate the combination of all CNM effects by a suppression factor,

$$S_{nuc} = \exp[-\rho_N \sigma_{abs} L(b)] , \quad (13)$$

with an effective nuclear absorption cross section,  $\sigma_{abs}$ . The latter will be considered over a range of 1-3.1 mb at RHIC and 0-2 mb at LHC. The former is compatible with the STAR measurement of  $R_{dAu} = 0.78 \pm 0.20 \pm 0.28$  for  $\Upsilon(1S+2S+3S)$  at RHIC [31], while CNM effects are expected to be reduced at LHC due to the much increased Lorentz contraction of the incoming nuclei. The other parameters in Eq. (13) are the nuclear density,  $\rho_N=0.14$  fm $^{-3}$ , and the impact-parameter dependent path length,  $L(b)$ , evaluated with a Glauber model for the nuclear overlap.

Current experimental limitations prevent resolving of individual  $\Upsilon(nS)$  states at RHIC and are reported as a combined cross section for  $\Upsilon(1S+2S+3S)$  including the  $\Upsilon(nS) \rightarrow e^+e^-$  branching ratios, i.e.,  $\sum_{n=1}^3 \mathcal{B}(nS)\sigma(nS)$  [41]. The measured value turns out to be consistent with next-to-leading order (NLO) color-evaporation model (CEM) calculations (using MRST HO parton distribution functions) for the individual  $\Upsilon$  production cross sections [33]. We therefore adopt the latter in our calculations, which are close to the values used in previous work [7].

To estimate the bottomonium cross sections at  $\sqrt{s_{NN}}=2.76$  TeV we start from the inclusive production of  $\Upsilon$  measured by CMS [34],  $\sigma_{pp \rightarrow \Upsilon}^{tot}(\sqrt{s}=7$  TeV,  $|y|<2) \simeq (300 \pm 40)$  nb (employing a  $\mu^+\mu^-$  branching ratio of  $B_{\mu\mu}=2.5\%$ ). Guided by NLO calculations [42] we extrapolate to 2.76 TeV by a factor of 0.5 and to full rapidity by a factor of 1/0.6. For a rapidity window of  $\Delta y=1.8$  for one thermal fireball ( $R_y=0.3$ , see below), we obtain  $\sigma_{pp \rightarrow \Upsilon}^{tot}(\sqrt{s}=2.76$  TeV,  $|y|<0.9) \simeq (75 \pm 8)$  nb. Alternatively, we can estimate this quantity by taking the CMS midrapidity value of

$d\sigma_{pp\rightarrow\Upsilon}/dy(\sqrt{s}=7\text{ TeV}) \simeq (80\pm 9)\text{ nb}$ , downscale it by a factor of 2 and multiply by  $\Delta y=1.8$  to obtain  $\sigma_{pp\rightarrow\Upsilon}^{\text{tot}}(\sqrt{s}=2.76\text{ TeV}, |y|<0.9) \simeq (72\pm 8)\text{ nb}$ , consistent with the above estimate. These estimates are also compatible with the CDF value [43] of  $d\sigma_{pp\rightarrow\Upsilon}/dy(\sqrt{s}=1.8\text{ TeV}) \simeq (27\pm 1.5)\text{ nb}$ , extrapolated to 2.76 TeV with a factor of  $\sim 4/3$ . Based on the inclusive  $\Upsilon$  production, we fix the cross sections for direct  $\Upsilon$ ,  $\Upsilon'$ , and  $\chi_b(1P)$  to maintain compatibility with the feeddown fractions given in Ref. [44] and listed in Tab. II; e.g., with a ca. 30% branching for  $\Upsilon' \rightarrow \Upsilon X$  one needs  $\sigma_{pp\rightarrow\Upsilon'} \simeq \frac{1}{3}\sigma_{pp\rightarrow\Upsilon}$  to obtain a feeddown fraction of  $\sim 10\%$ , and likewise for the  $\chi_b$  states.

The regeneration component requires the knowledge of the  $b\bar{b}$  cross section, which we also take from  $pp$  measurements together with binary-collision scaling. At RHIC the STAR measurement [36] gives  $\sigma_{pp\rightarrow b\bar{b}}^{\text{tot}}(\sqrt{s}=0.2\text{ TeV})=(1.6\pm 0.5)\mu\text{b}$ , where we combined statistical and systematic errors. This is slightly smaller than, but compatible with, the value of  $2\mu\text{b}$  used in Ref. [7]. The recent PHENIX measurements finds a larger central value [37],  $\sigma_{pp\rightarrow b\bar{b}}^{\text{tot}}(\sqrt{s}=0.2\text{ TeV})=(3.2\pm 1.8)\mu\text{b}$ , which, however, is still compatible with the STAR datum within combined statistical and systematic errors [46]. In our calculations below we will use a PHENIX value since it results in a  $\Upsilon/b\bar{b}$  ratio which is closer to the LHC value, but we will also comment on using the STAR value. At LHC our baseline value is obtained from LHCb data at 7 TeV [34], again downscaled by a factor of 2. With  $R_y=0.3$  for one thermal fireball (see below), one then finds  $\sigma_{pp\rightarrow b\bar{b}}(\sqrt{s}=2.76\text{ TeV}, |y|<0.9)\simeq(43\pm 8)\mu\text{b}$ . Alternatively, one can estimate this quantity by using the midrapidity values of  $(35\pm 5)\mu\text{b}$  at 7 TeV [34] and  $(15\pm 2)\mu\text{b}$  at 1.96 TeV [39] to extrapolate to  $\sim(20\pm 3)\mu\text{b}$  at 2.76 TeV (per unit rapidity), which, upon multiplying with  $\Delta y=1.8$ , yields  $\sigma_{pp\rightarrow b\bar{b}}(\sqrt{s}=2.76\text{ TeV}, |y|<0.9)\simeq(36\pm 5)\mu\text{b}$ , consistent with the above value. Since nuclear shadowing is believed to be significant at LHC, and applicable to the initial  $b\bar{b}$  production, a reduction factor of 0.75 will be included in Pb-Pb collisions (note that for  $\Upsilon$  states the shadowing effect is associated with the CNM suppression factor,  $S_{\text{nuc}}$ , in Eq. (13)). At RHIC, we assume no shadowing on initial  $b\bar{b}$  production.

As indicated above, a thermal fireball of light particles covers about 1.8 units in rapidity; the total number of initially produced  $Y$  (or  $b\bar{b}$ ) states within the fireball are thus obtained as

$$N_X(\tau_0) = \frac{\sigma_{pp\rightarrow X}^{\text{tot}}}{\sigma_{pp}^{\text{inel}}} N_{\text{coll}}(b) R_y S_{\text{nuc}} \quad (14)$$

with  $X = \Upsilon, \Upsilon', \chi_b, b\bar{b}$ ; here,  $R_y \simeq 0.52(0.3)$  denotes the fraction of the total number of  $X$  contained in  $\Delta y=1.8$  around midrapidity at RHIC (LHC). For  $X = b\bar{b}$ ,  $S_{\text{nuc}}=1(0.75)$  for RHIC (LHC).

To properly account for the observed inclusive  $\Upsilon$  yields, feeddown from higher bound states is computed. The

Prompt $\Upsilon(1s)$	$\sim 51\%$
$\Upsilon(1s)$ from $\chi_b(1P)$ decays	$\sim 27\%$
$\Upsilon(1s)$ from $\chi_b(2P)$ decays	$\sim 10\%$
$\Upsilon(1s)$ from $\Upsilon(2S)$ decays	$\sim 11\%$
$\Upsilon(1s)$ from $\Upsilon(3S)$ decays	$\sim 1\%$

TABLE II: The decomposition of the total (inclusive)  $\Upsilon(1s)$  yield into the direct  $\Upsilon$  and feeddown from excited states. The composition was determined from  $\sqrt{s_{NN}}=39\text{ GeV}$   $p$ - $p$  collisions [44].

magnitude of this contribution in  $pp$  collisions is given in Tab. II, reaching ca. 50% for the inclusive  $\Upsilon$  yield. We assume this to carry over to the initial conditions for AA collisions and solve individual rate equations for direct  $\Upsilon$ ,  $\Upsilon'$  and  $\chi_b$ ; we do not distinguish individual  $\chi_b$  states so that their combined feeddown amounts to 37% in  $pp$ ; the  $\Upsilon'$  contributes 11%. The feeddown from the  $\Upsilon''$  is considered negligible (1%). This decomposition of the total  $\Upsilon$  yield is assumed to be independent of the collision energy and colliding systems.

#### IV. COMPARISON TO DATA

Utilizing the previously discussed binding scenarios and dissociation mechanisms (Sec. II), implemented into the rate equation in a thermal-fireball background (Secs. III A and III B), observables are calculated for comparison to recent data at RHIC and LHC in the form of the nuclear modification factor,

$$R_{AA}(N_{\text{part}}) = \frac{N_Y^{AA}(N_{\text{part}})}{N_{\text{coll}}(N_{\text{part}}) \frac{\sigma_{pp\rightarrow Y}^{\text{tot}}}{\sigma_{pp}^{\text{inel}}} R_y} \quad (15)$$

The numerator,  $N_Y^{AA}$ , is the solution of the rate equation (7) at chemical freezeout. Deviations from unity are induced by CNM effects, suppression and regeneration in heavy-ion collisions. All previous studies of  $R_{AA}^Y$  thus far show suppression to be the dominant effect; significance of regeneration in the total yield was only suggested in our previous calculation [7] and in the statistical model [8] where all primordial bottomonia are assumed to be dissociated. In the following figures, our calculations for  $R_{AA}$  are broken up into nuclear absorption, primordial, and regeneration components, a luxury not available to experiment, but instructive for interpreting the data.

##### A. RHIC

As mentioned above our calculations at RHIC supplement previous work [7] for the same collision system, with slightly updated fireball, spectral-function and input parameters. In Fig. 7 we summarize our results for

the  $R_{AA}(N_{\text{part}})$  in 0.2 ATeV Au-Au collisions, for the combined  $\Upsilon(1S+2S+3S)$  (including  $e^+e^-$  branching ratios) [47] compared to STAR data in the upper row, and for the direct  $\Upsilon$ ,  $\Upsilon'$  and  $\chi_b$  in rows 2-4. The left panels, representing the weak-binding scenario, show substantial suppression, reaching a factor of  $\sim 2$  for the ground state and more than 5 for the excited states in central Au-Au. Regeneration does not play any role due to a small equilibrium limit, recall Fig. 5. The combined  $R_{AA}(1S+2S+3S)$  is in the lower parts of, but not inconsistent with, the STAR data. In the strong-binding scenario the suppression of the ground state is noticeably less pronounced than in the WBS, being almost entirely due to CNM effects. On the other hand, it might seem surprising that the suppression of the excited states is rather comparable in both scenarios. As discussed in Sec. II, this is due to the similar dissociation rates of  $Y(2S)$  and  $\chi_b(1P)$  in SBS and WBS at moderate QGP temperatures (recall Fig. 2), originating from the larger coupling and favorable dissociation kinematics in the gluo-dissociation processes (thus compensating the larger binding energy). This, in particular, puts into question a “sequential suppression pattern” (or “thermometer”) which is often discussed without taking into account the finite width of the bound states. The weaker suppression in the combined  $R_{AA}(1S+2S+3S)$  in the SBS relative to the WBS is thus mainly due the  $Y(1S)$ . This supports the assertion made in the original work [7] that the suppression level of the ground-state  $\Upsilon$  is the most sensitive observable for color screening. In the SBS, regeneration contributions are small but rather significant especially for the  $\chi_b$ , helped by its large inelastic reaction rate. They decrease by a factor of 2 upon decreasing the bottom cross section from  $3.2 \mu\text{b}$  (PHENIX central value) to  $1.6 \mu\text{b}$  (STAR central value), since bottom states are in the canonical limit at RHIC.

## B. LHC Results

Building upon previous  $Y$  calculations for the LHC in Pb-Pb collisions at  $\sqrt{s_{NN}}=5.5 \text{ TeV}$  [7] we examine the centrality dependence at  $\sqrt{s_{NN}}=2.76 \text{ TeV}$ , displayed in Fig. 8 for inclusive and direct  $\Upsilon$ , as well as for direct  $\Upsilon'$  and  $\chi_b$ . The higher temperatures at LHC (relative to RHIC) reinforce the stronger suppression in the weak-binding scenario compared to strong binding, for inclusive and direct  $\Upsilon$  production. The CMS data [11] are now significantly better described in the SBS, suggesting little effect of color-screening on the ground state even under LHC conditions. The initially (would-be) produced excited states exhibit close to complete suppression in both scenarios, but significant regeneration occurs in the SBS, due to a much larger equilibrium limit. This should be a measurable effect, especially in connection with  $p_t$  spectra (not discussed in our present work). In addition, the feeddown of the regenerated excited states accounts for a significant portion of the observed (inclusive)  $\Upsilon(1S)$  re-

generative component. Without feeddown, the regeneration effect is  $\sim 5\%$ , while including feeddown it is roughly twice as large,  $\sim 10\%$ . The understanding of the behavior of the higher  $\Upsilon'$  and  $\chi_b$  states is thus essential to a proper interpretation of the observed  $\Upsilon$  ground-state production at LHC.

## C. Comparison to Other Recent Work

In this section we briefly discuss the results from other recent calculations of  $Y$  production in URHICs in comparison to our findings.

In Ref. [9]  $Y$  suppression at RHIC was studied using gluo-dissociation with vacuum binding energies, folded over an ideal hydrodynamic evolution. Dissociation temperatures were implemented according to potential-model results based on  $V$  or  $U$  potentials. In line with our results for the SBS, the  $Y(1S)$  remains essentially unsuppressed in Au-Au( $\sqrt{s_{NN}}=0.2 \text{ TeV}$ ) collisions, while the yields and  $p_T$ -spectra of excited states show significant sensitivity to variations in the dissociation temperature. The larger dissociation temperatures following from  $V=U$  give results close to our SBS.

In Ref. [13]  $Y$  suppression was computed using an in-medium Cornell potential [18] including a perturbative imaginary part and the effect of anisotropies. The imaginary part corresponds to quasifree dissociation [22, 23], and was folded over an “extended anisotropic hydrodynamics” evolution. The resulting suppression in Pb-Pb at LHC is somewhat weaker than in our WBS, partly because the anisotropies decrease the  $Y$  dissociation rates.

In Ref. [14] the gluo-dissociation cross section was extended to approximately incorporate the string term in the  $b\bar{b}$  potential. With in-medium binding energies but with a rather small coupling constant of  $\alpha_s=0.2$ , a schematic estimate of the  $\Upsilon$  suppression in central Pb-Pb at LHC is roughly compatible with CMS data.

Close to completion of our work, Ref. [45] appeared where bottomonium production at RHIC and LHC is computed within the same rate-equation approach [7, 26] as employed here, including regeneration. The  $Y$  dissociation widths were taken from a NLO perturbative QCD calculation folded over a schematic viscous fireball evolution with an ideal-gas equation of state. No constraints from lattice correlators on the  $Y$  spectral functions were evaluated. Contrary to our results, a preference for an in-medium binding scenario has been inferred and no significant regeneration contributions are found even at LHC.

## V. CONCLUSIONS

We have studied bottomonium production in ultrarelativistic heavy-ion collisions at RHIC and LHC utilizing a kinetic rate-equation approach in a quark-gluon plasma background, including suppression and regeneration mechanisms dictated by detailed balance. Our cal-



culations are based on previous work in Ref. [7] where, in particular, two scenarios for bottomonia in the QGP were evaluated, i.e. vacuum and in-medium bound-state properties (vis-a-vis strong and weak-binding scenarios). At the time, the latter seemed to be the theoretically better motivated case. The present work, however, suggests a re-evaluation of this view. Firstly, the strong-binding limit provides a more natural explanation of the near temperature independence of bottomonium correlators now available from thermal lattice QCD. Furthermore, the application to recent STAR and CMS data at RHIC and LHC (including updated open and hidden-bottom input cross sections) indicates that a more stable  $\Upsilon$  ground state gives a better description of its nuclear modification factor. These findings corroborate the picture that the  $\Upsilon$  ground state is not much affected by color screening up to fairly high temperatures of  $\sim 3-4T_c$ . We also found that regeneration contributions, which have been neglected in most previous works, are not negligible, especially for strong binding at the LHC.

Several lines of future studies emerge. The background medium needs to be improved using realistic hydrody-

namic evolutions. Some work in this direction has already been conducted. The regeneration term should be calculated with time-dependent bottom-quark spectra, constrained by  $B$ -meson observables. Based on those, transverse-momentum spectra and elliptic flow of bottomonia need to be calculated (again, pertinent work has begun). In all these, the consistency to the charmonium and open-charm sector should be maintained. A comprehensive description of heavy-flavor observables, based on theory constrained by lattice QCD, remains the long-term goal, which appears to be achievable.

### Acknowledgments

This work was supported in part by the National Science Foundation (NSF) grant No. PHY-0969394 (RR), the Department of Energy grant no. DE-FG02-87ER40371 (XZ), the Texas A&M Cyclotron Institute REU program under NSF grant No. PHY-1004780 (AE), and by the Humboldt Foundation (RR).

- 
- [1] R. Rapp, D. Blaschke and P. Crochet, *Prog. Part. Nucl. Phys.* **65**, 209 (2010).
  - [2] L. Kluberg and H. Satz, arXiv:0901.3831 [hep-ph].
  - [3] P. Braun-Munzinger and J. Stachel, arXiv:0901.2500 [nucl-th].
  - [4] J.F. Guion and R. Vogt, *Nucl. Phys.* **B492**, 301 (1997).
  - [5] D. Pal, B. K. Patra and D.K. Srivastava, *Eur. Phys. J. C* **17**, 179 (2000).
  - [6] V.P. Goncalves, *Phys. Lett.* **B518**, 79 (2001).
  - [7] L. Grandchamp, S. Lumpkins, D. Sun, H. van Hees, R. Rapp, *Phys. Rev. C* **73**, 064906 (2006).
  - [8] A. Andronic, P. Braun-Munzinger, K. Redlich, J. Stachel, *Nucl. Phys.* **A789**, 334 (2007).
  - [9] Y. Liu, B. Chen, N. Xu and P. Zhuang, *Phys. Lett.* **B697**, 32 (2011)
  - [10] S. Chatrchyan *et al.* [CMS Collaboration], *Phys. Rev. Lett.* **107**, 052302 (2011).
  - [11] The CMS Collaboration, Physics Analysis Summary HIN-10-006 (2011), *Quarkonium production in PbPb collisions at  $\sqrt{s_{NN}}=2.76$  TeV*; <http://cdsweb.cern.ch/record/1353586/files/HIN-10-006-pas.pdf>.
  - [12] R. Reed *et al.* [STAR Collaboration], arXiv:1109.3891 [nucl-ex].
  - [13] M. Strickland, *Phys. Rev. Lett.* **107**, 132301 (2011)
  - [14] F. Brezinski and G. Wolschin, arXiv:1109.0211 [hep-ph].
  - [15] A. Jakovac, P. Petreczky, K. Petrov and A. Velytsky, *Phys. Rev. D* **75**, 014506 (2007).
  - [16] G. Aarts, S. Kim, M.P. Lombardo, M.B. Oktay, S.M. Ryan, D.K. Sinclair, J.-I. Skullerud, *Phys. Rev. Lett.* **106**, 061602 (2011).
  - [17] G. Aarts *et al.*, arXiv:1109.4496 [hep-lat].
  - [18] F. Karsch, M.T. Mehr and H. Satz, *Z. Phys. C* **37**, 617 (1988).
  - [19] X. Zhao and R. Rapp, *Phys. Rev. C* **82**, 064905 (2010).
  - [20] F. Riek and R. Rapp, *Phys. Rev. C* **82**, 035201 (2010).
  - [21] M.E. Peskin, *Nucl. Phys.* **B156**, 365 (1979); G. Bhanot and M.E. Peskin, *Nucl. Phys.* **B156**, 391 (1979).
  - [22] L. Grandchamp and R. Rapp, *Phys. Lett.* **B523**, 60 (2001).
  - [23] F. Riek and R. Rapp, *New J. Phys.* **13**, 045007 (2011).
  - [24] N. Brambilla, M.A. Escobedo, J. Ghiglieri and A. Vairo, arXiv:1109.5826 [hep-ph].
  - [25] M. Laine, O. Philipsen, P. Romatschke, M. Tassler, *JHEP* **0703**, 054 (2007).
  - [26] L. Grandchamp, R. Rapp and G.E. Brown, *Phys. Rev. Lett.* **92**, 212301 (2004).
  - [27] R. Rapp and H. van Hees, in *Quark-Gluon Plasma 4* (R. Hwa and X.N. Wang, eds.), World Scientific (Singapore), 111 (2010); and LANL eprint arXiv:0903.1096 [hep-ph].
  - [28] L. Grandchamp and R. Rapp, *Nucl. Phys.* **A709**, 415 (2002).
  - [29] H. van Hees, M. Mannarelli, V. Greco and R. Rapp, *Phys. Rev. Lett.* **100**, 192301 (2008).
  - [30] X. Zhao and R. Rapp, *Nucl. Phys.* **A859**, 114 (2011).
  - [31] H. Liu *et al.* [STAR Collaboration], *Nucl. Phys.* **A830**, 235C (2009); R. Reed *et al.* [STAR Collaboration], *Nucl. Phys.* **A855**, 440 (2011).
  - [32] S. Eidelman *et al.* (Particle Data Group), *Phys. Lett.* **B592**, 1 (2004).
  - [33] A. D. Frawley, T. Ullrich, and R. Vogt, *Phys. Rep.* **462**, 125 (2008).
  - [34] V. Khachatryan *et al.* [CMS Collaboration], *Phys. Rev. D* **83**, 112004 (2011).
  - [35] R. Vogt, *Phys. Rev. C* **81**, 044903 (2010).
  - [36] Wenqin Xu *et al.* [STAR Collaboration], arXiv:1106.6020 [nucl-ex].
  - [37] A. Adare *et al.* [PHENIX Collaboration], *Phys. Rev. Lett.* **103**, 082002 (2009).

- [38] LHCb Collaboration, Phys. Lett. **B694**, 209 (2010).
- [39] D. Acosta *et al.* [CDF Collaboration], Phys. Rev. D **71**, 032001 (2005).
- [40] R. Vogt (Hard Probe Collaboration), Int. J. Mod. Phys. **A696**, 669 (2003).
- [41] B.I. Abelev *et al.* [STAR Collaboration], Phys. Rev. D **82**, 012004 (2010).
- [42] R. Vogt, Eur. Phys. J. C **61**, 793 (2009).
- [43] D. Acosta *et al.* [CDF Collaboration], Phys. Rev. Lett. **88**, 161802 (2002).
- [44] T. Affolder *et al.* (CDF Collaboration), Phys. Rev. Lett. **84**, 2094 (2000).
- [45] T. Song, K.C. Han and C.M. Ko, arXiv:1109.6691 [nucl-th].
- [46] The PHENIX measurement of the total  $b\bar{b}$  cross section is based on the midrapidity datum of  $d\sigma_{pp}^{b\bar{b}}/dy=(0.92\pm 0.5)\mu\text{b}$ ; the extrapolation to the total is consistent with our rapidity-coverage factor of  $\Delta y/R_y=1.8/0.52=3.46$ , see Eq. (14), as originally inferred in Ref. [7]
- [47] The branching ratios are taken from Ref. [33]; the suppression pattern of the 3S state is approximated as following the 2S one.

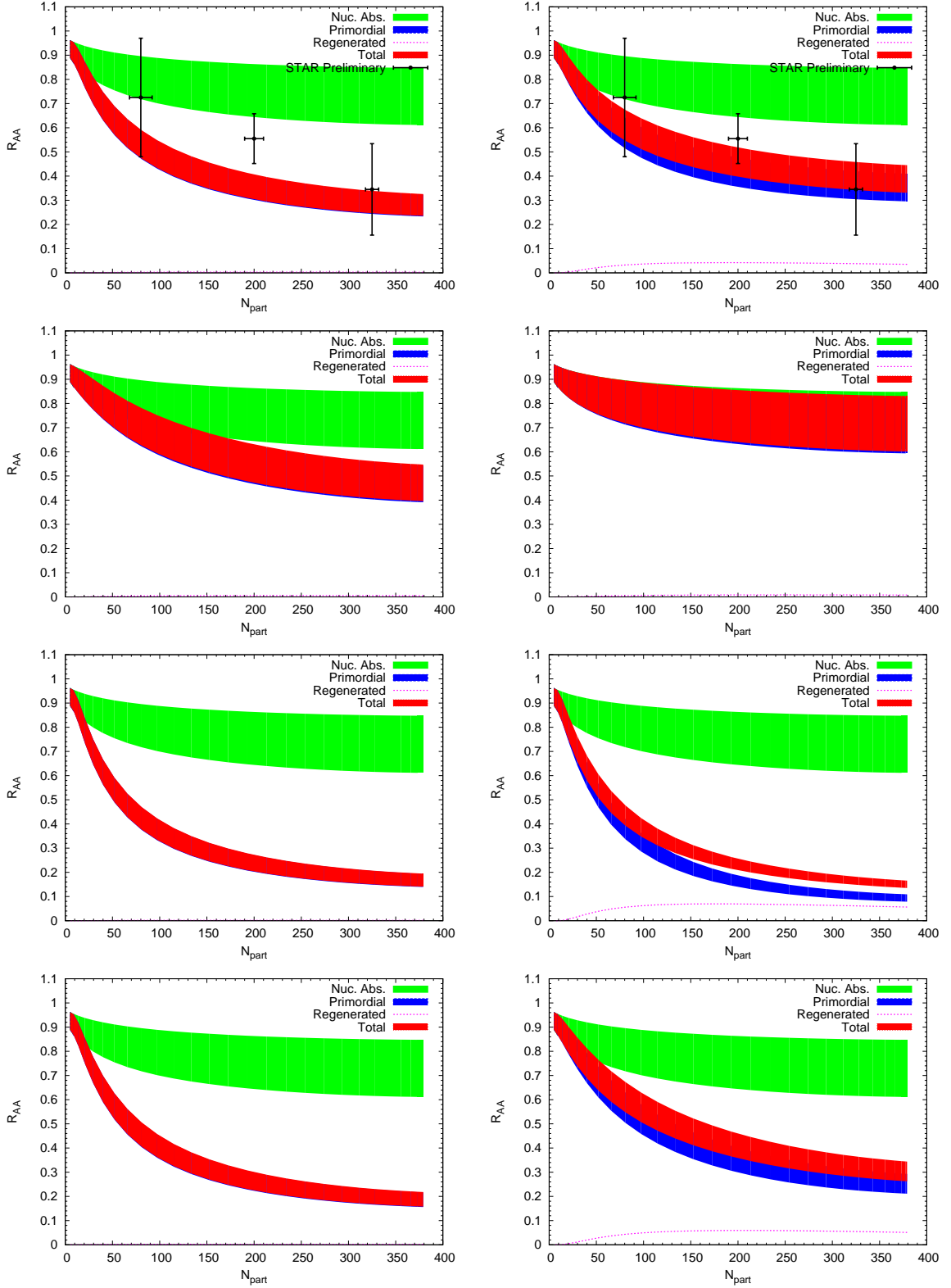


FIG. 7: The nuclear modification factor for  $\Upsilon(1S+2S+3S)$  including  $e^+e^-$  branching (top row, compared to STAR data [12]), direct  $\Upsilon$  (second row),  $\Upsilon'$  (third row) and  $\chi_b$  (bottom row), as a function of centrality in Au-Au( $\sqrt{s_{NN}}=0.2$  TeV) collisions at RHIC. The left column corresponds to the weak-binding scenario, the right one to the strong-binding scenario. In each panel, CNM effects alone are shown by the green band, CNM plus QGP suppression by the blue band, regeneration by the dashed pink line and the total by the red band. If regeneration is small, red and blue bands largely overlap.

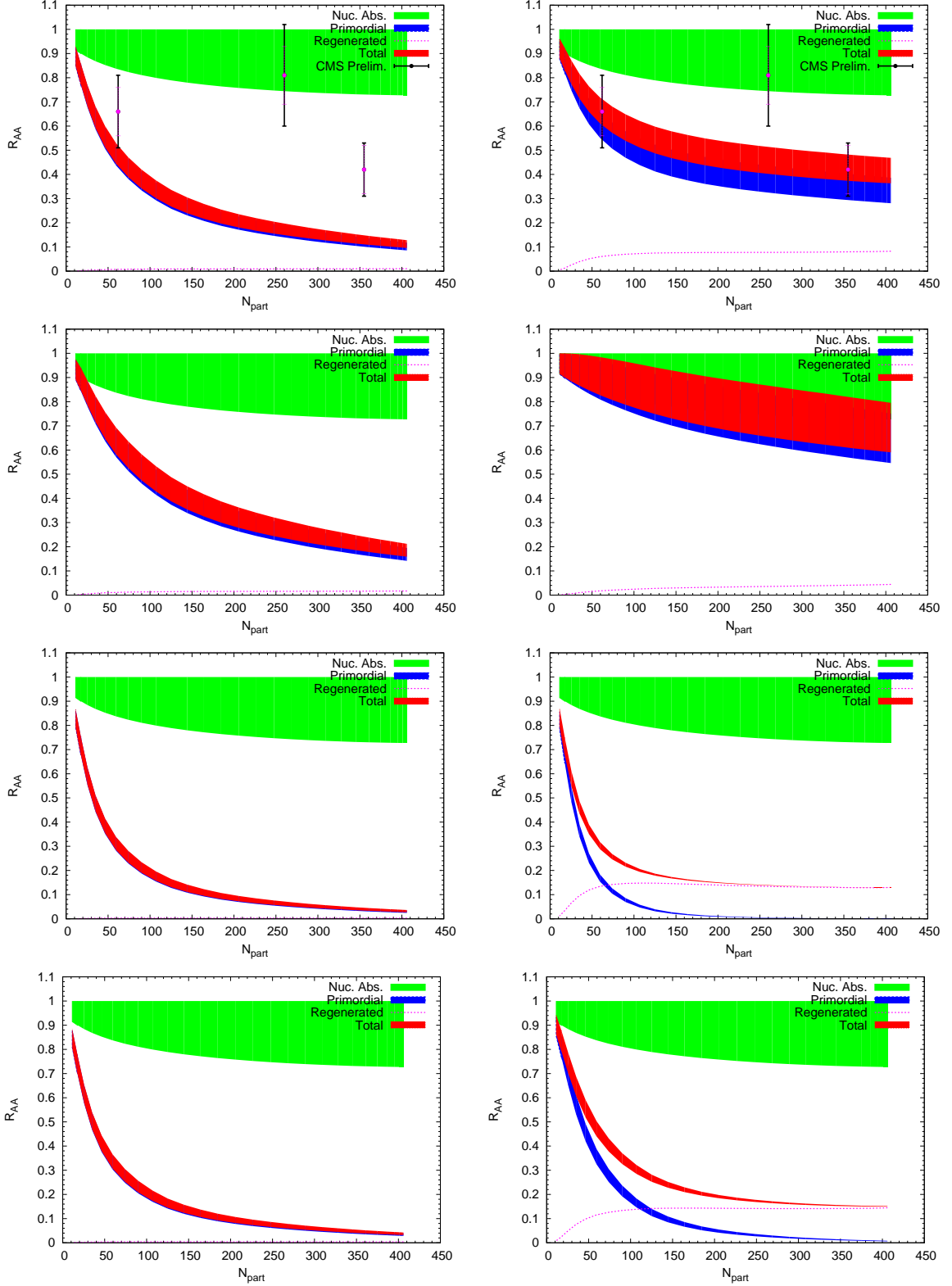


FIG. 8: The nuclear modification factor for inclusive  $\Upsilon$  (top row, compared to CMS data [11]), direct  $\Upsilon$  (second row),  $\Upsilon'$  (third row) and  $\chi_b$  (bottom row), as a function of centrality in Pb-Pb( $\sqrt{s_{NN}}=2.76$  TeV) collisions at LHC. The left column corresponds to the weak-binding scenario, the right one to the strong-binding scenario. In each panel, CNM effects alone are shown by the green band, CNM plus QGP suppression by the blue band, regeneration by the dashed pink line and the total by the red band.